ResearchGate

See discussions, stats, and author profiles for this publication at: https://www.researchgate.net/publication/231648935

Toward Understanding of the Propulsion Mechanism of Rod-Shaped Nanoparticles That Catalyze Gas-Generating Reactions

ARTICLE *in* THE JOURNAL OF PHYSICAL CHEMISTRY C · MARCH 2008

Impact Factor: 4.77 · DOI: 10.1021/jp710594w

CITATIONS
31

READS
37

1 AUTHOR:

N. I. Kovtyukhova
Pennsylvania State University
33 PUBLICATIONS **2,810** CITATIONS

SEE PROFILE

Available from: N. I. Kovtyukhova
Retrieved on: 01 February 2016

Toward Understanding of the Propulsion Mechanism of Rod-Shaped Nanoparticles That Catalyze Gas-Generating Reactions

Nina I. Kovtyukhova[†]

Department of Chemistry, The Pennsylvania State University, University Park, Pennsylvania 16802

Received: November 5, 2007; In Final Form: February 19, 2008

There is no consensus in the literature on the propulsion mechanism of rod-shaped nanomotors that catalyze hydrogen peroxide decomposition to oxygen and water. Historically, the directional motion was discovered with bimetallic nanorods,[1,2] and the related asymmetry of catalytic rod surface has been taken as a necessary condition of self-propulsion in all of the mechanisms proposed to date. This study for the first time demonstrates that hydrodynamic behavior of monocomponent catalytic nanorods in a H_2O_2 solution is similar to that of the bicomponent ones, and hence, the surface chemical asymmetry is unlikely to be a governing factor in the rods self-propulsion. The experimental results have shown that oxygen bubbles' evolution from the rod surface and related gravitational forces alone can drive directional motion of the rods. A new model is proposed that is based on the gravitational forces and considers rod motion in the 3D space. Nonparallel rods orientation relative to the horizontal plane has been found to play a major role in rods propulsion. Momentum exchange between such a "tilted" rod and water flux, caused by the oxygen bubbles' departure, drives the rod propulsion. The proposed mechanism provides a reasonable explanation for all behavior patterns of the nanorod motors. Motility of Pt and Rh nanorods was studied in the rod length range of 2−7 μm and the H_2O_2 concentration range of 3−30 wt %. Confocal microscopy was used to estimate nanorods orientation relative to the horizontal plane.

1. Introduction

The continual effort to gain useful mechanical work from chemical energy sources has now reached down to the micro- and nanoscale. Several recent findings have demonstrated that chemical energy can be converted into kinetic energy of the directional motion of micron and submicron particles,[1−5] thus opening the era of synthetic nanomotors.

Understanding and exploiting of chemically driven nano-(micro)motors could benefit from accumulated knowledge of both the biological chemical-to-mechanical energy conversion systems and the macroscale combustion engines. Micron-size animals demonstrate elegant strategies of swimming at low Reynolds numbers by mechanical deformations of their body. Energy of a chemical process running inside the body converts into the mechanical energy of these deformations. Interaction of the continuously deforming body with a surrounding fluid causes the body propulsion.[6a,b] Implementation of such strategies with synthetic swimmers requires geometric asymmetry and flexibility of their body structure.[6c] This, for example, can be achieved using particle ensembles. A chain of colloidal particles linked with DNA can act as a flexible flagellum when attached to a blood cell.[7] This system, however, is driven by magnetic forces and does not convert chemical energy.

When synthetic swimmers are rigid single-particle devices, useful body deformations are hardly possible, and the propulsion is enabled by a chemical reaction that occurs outside the body in a surrounding fluid and on the external body surface.[1−5,8−11] Nano(micro)motors of this type rather exploit the concept of a combustion engine, where change in the energy balance of the fluid phase causes displacement of the movable solid parts.[5] Decomposition of chemical fuel (such as hydrogen peroxide or ethanol) to gas and water on the catalytic surface of moving objects was shown to cause propulsion of small particles in a solution[1−4] and fluctuating of microcantilevers.[5]

It is common knowledge that, in the systems containing gas bubbles and solid particles dispersed in a liquid, density differences drive much of the hydrodynamic behavior due to gravity. While it is believed that oxygen bubbles' formation and the related gravitational forces are responsible for the propulsion of the macro/micro-objects in H_2O_2 solutions,[2,3,8,9] several alternate hypotheses that disregard gravity effect have emerged at the nanoscale.[1,4,12,13] In the case of rod-shaped nanomotors, which are currently represented in the literature by bimetallic nanorods, the proposed mechanisms rely on the formation of a surface tension gradient[1] or electrochemical potential difference[12,13] along the rod length. Verification of these hypotheses, however, remains a challenge for several fundamental reasons:

(i) The proposed mechanisms ignore oxygen bubbles' formation on and departure from the rod surface and the related gravitational forces exerted on the rod body, although very strong competing gravity effect can suppress the effect of other forces on fluid behavior.[14]

(ii) They consider only two-dimensional rod motion (i.e., the rod body is always parallel to the horizontal plane), which is not normally the case of colloidal rods dispersions.[15]

(iii) They are restricted to the asymmetric catalytic surfaces of bimetallic rods and cannot explain the propulsion of monocomponent rods. The bipolar electrochemical mechanism, in addition, requires the formation of well-organized proton double layer along the rod surface[12,13] that is difficult to expect in the case of metal−H_2O_2 complex formation, presence of free

[†] E-mail: nina@chem.psu.edu.

10.1021/jp710594w CCC: $40.75 © 2008 American Chemical Society
Published on Web 03/27/2008

radical species, and oxygen evolution from the surface, which all take place during the catalytic H_2O_2 decomposition on metal surfaces.

It has now become clear that thorough consideration of all forces acting in the system is a necessary next step toward understanding of the underlying principles of the rods self-propulsion, which is needed for practical realization of the existing devices and discovery of new systems. The goal of our paper is to contribute to this understanding by presenting a new model based on experimental and theoretical examination of a contribution of the gravitational forces to self-propulsion of catalytic rod-shaped nanoparticles that generate oxygen bubbles' formation in aqueous H_2O_2 solutions. These forces are expected to play a dominant role in the systems based on gas-producing reactions, where effect of other forces becomes much less significant.

We have studied a simple case of symmetric monocomponent metal rods that catalyze H_2O_2 decomposition to oxygen and water. This approach allows eliminating alternate effects that may arise from differences in surface properties of the asymmetric bicomponent rods (such as hydrophobicity,[1] catalytic activity,[2] and redox potential[12,13]).

Another distinctive feature of our approach is the consideration of rod motion in the three-dimensional space to account for gravitational forces. It is important to note that conventional wide-field microscopy, which has most commonly been used for tracking the motion of nano(micro) rods in a solution, gives a two-dimensional image of the system, which does not allow determining rod orientation relative to the direction of gravity. Here we show that rods orientation in the 3D space is crucial for understanding of their hydrodynamic behavior.

It has been found that the rate of oxygen formation on the rod surface, geometric parameters of the rod, and the angle that rod's long axis makes with the horizontal plane mainly determine the hydrodynamic behavior of the system. We have observed that the monocomponent Pt and Rh rods exhibit the same behavior patterns as bimetallic rods.[1,2] This implies that asymmetry of the catalytic surface is not the governing factor in self-propulsion, and hence, the second component (less active) is not needed to enable directional movement of the rod-shaped nanoparticles. The proposed gravitational model based on these findings provides a reasonable explanation for all behavior patterns of the monocomponent rods and may be extended to the bicomponent ones.

2. Experimental Methods

Pt and Rh nanorods were prepared by a routinely used technique of electrochemical replication of the cylindrical pores (diameter $\sim 350 \pm 20$ nm) of commercial alumina membranes (Anodisc 25, 0.2 μm). Electroplating of the rods was performed in potentiostatic mode at -0.25 V (Pt) and -0.45 V (Rh) vs SCE using commercial electroplating solutions Platinum TP and Techni Rhodium. The backside of a membrane was coated with Ag film, and $\sim$10 μm long Ag rods were electroplated inside the pores to fill their branched part. The membrane was thoroughly washed with water to remove the Ag solution from the pores, and Pt or Rh was then electroplated on top of the Ag rods. Pt and Rh rods were released into solution by dissolving the silver film and rods and the membrane in aqueous HNO_3 (1:1) and NaOH (0.5 M), respectively. Pt and Rh rods were thoroughly washed/centrifuged with deionized water and used as aqueous suspensions of pH $\sim$ 5.

Chemical composition of the rods was analyzed by inductively coupled plasma−atomic emission spectrometry (ICP), X-ray photoelectron spectroscopy (XPS), and Auger electron spectroscopy (AES). Analysis of Pt rods by ICP revealed Ag/Pt atomic ratio of $\sim$0.6%. However, XPS and AES analysis found Ag/Pt atomic ratio of $\sim$10%. These facts suggest that Ag is mainly located in subsurface layer (5−10 nm) and, according to AES, is relatively uniformly distributed along the rod length. A 10 min treatment of the Pt rods suspension with aqueous HNO_3 (1:1) or H_2O_2 (30%) did not release detectable amounts of Ag ($<$0.02 ppm by ICP) into a solution. This implies that there are no appreciable silver phase inclusions on the Pt rod surface exposed to a solution, and Ag is probably dispersed at the atomic level in the subsurface layer.

On the basis of the results of elemental analysis, it should be noted that the term "monocomponent", which is applied to Pt and Rh rods in this study, emphasizes chemical homogeneity of the catalytic surface along the rod body rather than the bulk composition of the rods. (The presence of some amount of silver in metal rods is probably an inevitable evil when those rods are electroplated on top of the Ag plugs inside the pores of an alumina membrane.)

Dynamic characteristics of the rods were studied in the H_2O_2 concentration range of 3−30% and the rod length range of 2−7 μm. Compared to the previous works, higher H_2O_2 concentrations were used to enable appreciable directional motion of nanorods longer than 3 μm. In a typical experiment, a very dilute suspension of the rods in aqueous H_2O_2 was injected into a perfusion chamber (19 $\times$ 6 $\times$ 0.5 mm, CoverWell PC4L-0.5, GRACE Bio-Labs) placed onto the microscope stage. During microscope focusing, the rods have enough time to settle within the 0.5 mm thick solution layer and can be considered in the state of sedimentation equilibrium by the beginning of observation of their motion. High dilution of the investigated suspensions allowed distances between the rods considerably larger than their lengths, and all measurements were made for the rods that were far away from the chamber walls. Under such experimental conditions, rod−rod and rod−wall interactions are negligible and do not noticeably affect rods orientation and motility. Rods motility was characterized in terms of center-to-center displacement speed (U_{Dr}), directionality (cosine of the angle that rods long axis makes with the direction of its movement), and axial velocity (product of the speed and directionality).[1] Trajectories of rods motion were tracked by analyzing video clips with the PhysVis program (Kenyon College).

Confocal microscopy images were taken in reflective mode using the Olympus FV300 laser scanning confocal microscope (Olympus America Inc.): laser: HeNe (543 nm); objective: 60$\times$ PlanApo; focal plane thickness: 0.2 μm. Similar perfusion chambers were used to accommodate aqueous rods suspensions of the same rods concentration.

Transmission electron microscopy (TEM) images were obtained with a JEOL 1200 EXII instrument at 80 kV accelerating voltage.

3. Results

Behavior of the monocomponent Pt and Rh nanorods in aqueous H_2O_2 solutions has much in common with that of bicomponent metal nanorods. Figure 1a−c shows three typical motion trajectories of the single Pt rods: relatively linear (a), circular (b), and radial (c). Ensembles of two crossed Pt rods rotate around the cross-point (Figure 1d) (see also Supporting Information movies 1−3). All these trajectory types have previously been reported for the bicomponent rods catalyzing H_2O_2 decomposition to oxygen and water.[1,2] Speed (U_{Dr}) and

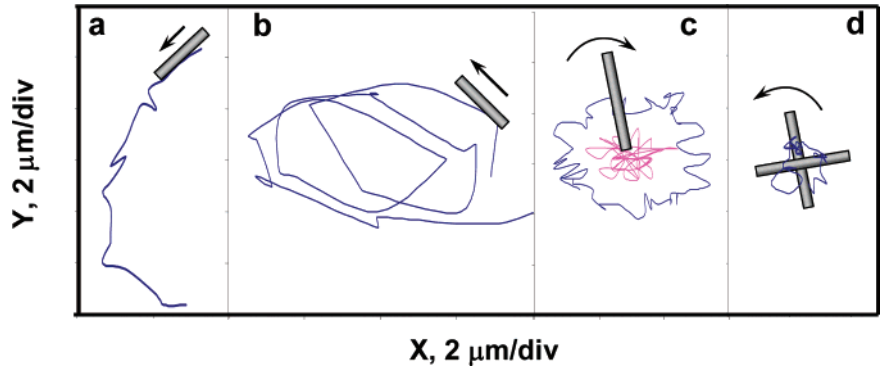

Figure 1. Trajectories of motion of Pt nanorods in an aqueous H_2O_2 solution. All of the trajectories are calculated for the rod center of mass. In (c), the trajectory for the lower rod end is also shown (pink line). The latter indicates that the rod lower end is not irreversibly bound to the surface but rather is very close to it, which slows down the linear motion and creates favorable conditions for developing alternate radial motion. In this experiment the rods were first cast onto a glass slide, and then a H_2O_2 solution was added.

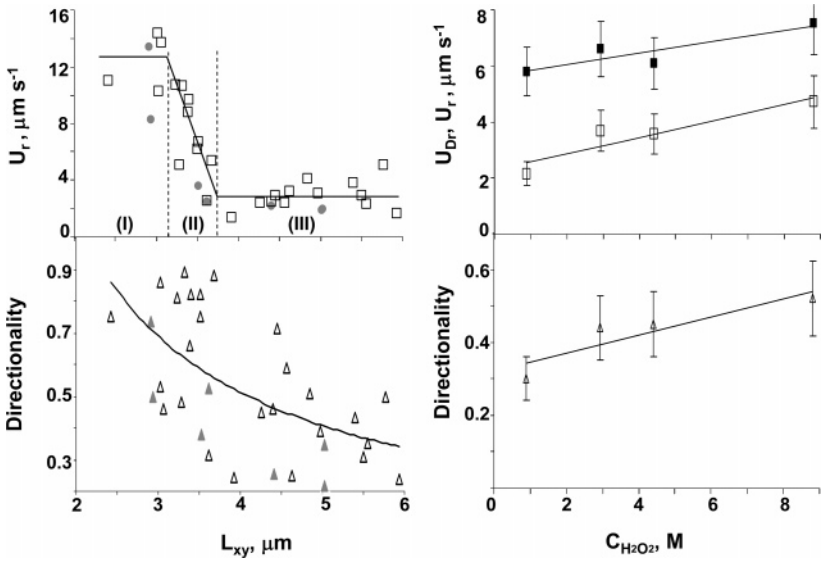

Figure 2. Dependencies of axial velocity and directionality on rod length (left) and H_2O_2 concentration (right). L_{xy} is a projection of rod length L onto the XY-plane. Data on the left were obtained for Pt (open squares and triangles) and Rh (solid circles and triangles) rods; lines are guides for eye. Data shown on the right were obtained for ~4.5 μm long Pt rods; solid squares show center-to-center displacement speed (U_{Dr}); each data point is averaged for 10−15 rods.

axial velocity (U_r) of the Pt and Rh nanorods are comparable to those of the bimetallic rods.[1,13]

Rods speed, axial velocity, and directionality are found to increase linearly with H_2O_2 concentration in the range of 3−30 wt % (Figure 2, right), which allows to suggest that these parameters are dependent on rate of oxygen evolution from the rod surface. It also indicates that higher oxygen bubbles' concentration in a bulk solution, which is expected at higher H_2O_2 concentrations, does not disrupt directional motion of the rods. An increase in speed and directionality with H_2O_2 concentration was observed for bimetallic rods as well.[1]

The dependence of the dynamic characteristics on rod length (L) is much more complex (Figure 2, left). The plot of the axial velocity vs L can be roughly divided into three regions: (I) ~2−3.2 μm long rods exhibit high velocity seemingly independent of L; (II) dramatic velocity drop in the rod length range of ~3.2−3.8 μm; (III) low velocity independent of L for 4−6 μm long rods. For both Pt and Rh rods, the directionality tends to decrease with the rod length.

The graph shapes shown in Figure 2 (left) are difficult to explain if rods motion is considered in the two-dimensional space, in which case axial velocity should be inversely proportional to rod length.[1,16] Also, the 2D diffusion coefficients of metal rods in water, characteristic of Brownian motion, were reported to decrease with rod length,[17] which implies that the poorer directionality of the longer rods is not caused by increasing contribution of the Brownian component.

For understanding of the propulsion mechanism, rods orientation in the three-dimensional space has to be taken into consideration. Subjected to the gravity force and Brownian motion, axisymmetric rod-shaped particles are randomly oriented in a solution with their long axes parallel neither to the direction of gravity nor to the bottom of the cell. It is known that, in general, nonspherical particles do not settle in the direction of gravity.[15,16] For the noninteracting rods, the sedimentation velocity vector can be written as $\mathbf{u}_{sed} = -\Delta\rho V\mathbf{g}\mathbf{f}^{-1}$, where $\Delta\rho$ is the density difference between the rod and the fluid, V the rod volume, $\mathbf{g}$ the acceleration vector in the direction of gravity, and $\mathbf{f}$ the resistance tensor. As an axisymmetric particle, a rod settles in a plane formed by its axis of revolution and the direction of gravity. Expressing $\mathbf{f}$ in space-fixed coordinates yields a set of equations from which it follows that the rod settles in a direction making a certain angle with the direction of gravity (for details see refs 15 and 16). This angle, in turn, is a function of an angle (θ) between the axis of revolution (long axis) of the rod and the XY-plane. As it is noted in the Experimental Section, observation of the catalysis-induced directional motion of the rods was started after their sedimentation had been

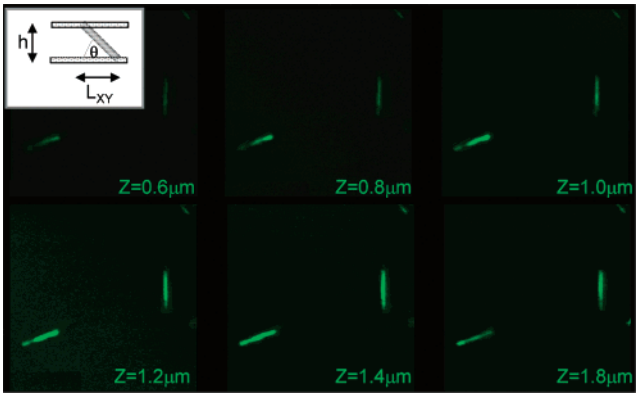

Figure 3. A typical *Z*-stack confocal microscopy image of a Pt rods aqueous suspension on a cover glass slide that was used for rough estimating the angle θ, which the rod long axis makes with the *XY*-plane. The rod shown on the left is "tilted" that is indicated by a brightness switch of the rod ends while the focal plane is moving up. $\tan\theta = h/L_{xy}$, where h is the vertical distance between the focal planes focused on the lower and upper ends of the rod (1 and 6, respectively) and L_{xy} is the length of the rod projection onto the *XY*-plane (see inset). The rod shown on the right is almost parallel to the *XY*-plane but is not in contact with the glass slide. The rods exhibit some Brownian motion but maintain the angle with the glass slide.

completed. The rods are suggested to reach the state of sedimentation equilibrium and maintain their angle with the *XY*-plane. (Sedimentation, therefore, should not significantly affect the rods directional motion, and it is not further considered in this study.) Existence of the rods "tilt" is confirmed by the facts that the moving rods always look shorter than those at rest, and one of the rod ends always look brighter (i.e., it is in focus) than the other. The angle between the rod body and the glass slide, θ, can be experimentally estimated using confocal microscopy imaging of nanorod suspensions in water, as shown in a representative image in Figure 3. Determining the vertical distance between focal planes that are focused on the lower and upper ends of the tilted rod allows to estimate θ. About 70% of the rods that are not in contact with the glass slide appear to be tilted. Very low rods concentration in the suspensions (i.e., large distances between the rods) suggests that their orientation is not noticeably affected by the presence of the neighboring particles.

It has been found that θ dependence on rod length is also complex and the graph shape is qualitatively similar to that of u_r vs L dependence. The θ vs L graph also can be roughly divided into three regions. In the L range of ~3−4.4 μm, θ values do not change with the rod length and are randomly scattered within the range of 26°−32° (region I). As rod length increases from ~4.4 to ~5.6 μm, a significant decrease in θ value is observed (region II). For longer rods, θ again becomes independent of L and remains in the range of 11°−15° (region III). It is to note that θ may be slightly different in water and in the oxygen-evolving H_2O_2 solution.

4. Discussion

Our analysis of hydrodynamics of the monocomponent catalytic nanorods in a H_2O_2 solution relies on the following statements derived from the experimental and literature data:

1. H_2O_2 decomposition on metallic (M) nanorod surface (walls and ends) is a free-radical process,[18] which may include the following reactions:[19,20]

$$M + H_2O_2 \rightarrow M(I) + HO^{\bullet} + HO^{-}$$

$$M(I) + H_2O_2 \leftrightarrow [M(I) - H_2O_2] \rightarrow M + HO_2^{\bullet} + H^{+}$$

$$M + HO^{\bullet} \rightarrow M(I) + HO^{-}$$

$$M(I) + HO_2^{\bullet} \rightarrow M + O_2 + H^{+}$$

$$H_2O_2 + HO^{\bullet} \rightarrow H_2O + HO_2^{\bullet}$$

$$HO^{\bullet} + HO_2^{\bullet} \rightarrow H_2O + O_2$$

Apparently, oxygen formation can simultaneously occur on the catalyst surface and in the bulk solution. Molecular oxygen then coalesces into bubbles that grow on the nanorod surface and depart due to buoyancy force. While direct observation of the bubbles on the surface of short moving nanorods is challenging, they can be clearly seen when H_2O_2 solution is cast on longer nanorods resting on the glass slide surface (see Supporting Information movie 4). After the bubbles depart from the surface, water emerges to fill their place and push the rod. This push is the driving force of the rod propulsion.

2. Useful information about bubbles' behavior can be obtained by watching O_2 evolution on the surfaces of larger wires (300 μm thick Pt and 100 nm thick Ni wires) immersed in a H_2O_2 solution (see, e.g., Supporting Information movie 5). We assume the similar behavior pattern for the much smaller bubbles on the nanorods surface. In particular, we observed the following:

(i) Direction of the bubbles' motion at the moment of departure is always normal to the surface. It means that, when the surface is curved or tilted, the bubbles do not move vertically upward at the very moment of separation. Only after the bubbles are free, their motion becomes vertical.

(ii) Size of the departing bubbles varies from microns to hundreds of microns and apparently does not depend on wire diameter. Sometimes it can considerably exceed diameter of the wire.

(iii) The less active surfaces (e.g., Ni vs Pt) tend to form much larger and slower growing bubbles.

(iv) The bubbles repeatedly grow on and depart from the same spots on the surface, which is consistent with bubble nucleation on surface defects (cavities) rather than on real catalytic sites responsible for oxygen formation. The high-resolution TEM image in Figure 5 shows that the rod walls are not ideally smooth, and nanocavities are likely to exist.

Similar bubbles' behavior has been observed for oxygen evolution on catalyst-coated SiO_2 microparticles[9] and gas or vapor evolution during electrolysis and boiling.[21]

3. The rods are in the state of sedimentation equilibrium, and their long axis makes an angle, θ, with the *XY*-plane, as shown schematically in Figure 6a. Considering forces acting on the oxygen bubbles and the rod body, one can see that such a "tilt" is responsible for existence of a force component directed parallel to the *X*,*Y*-plane, which enables the directional motion of the rod observed with a microscope. This phenomenon is discussed in greater detail below. If a rod is oriented parallel to the *XY*-plane, bubbles departing from the walls do not generate driving force along the rod long axis. Forces arising at the rod tips are mutually compensated. Thus, the parallel orientation does not favor rod directional motion (Figure 6b).

Gravitational Model. Balance of forces exerted on a departing O_2 bubble can be expressed as

$$F_b = V_{bO_2}\rho_{O_2}(u_{bst} - u_{b0})/\Delta t = gV_{bO_2}\rho_{H_2O} - gV_{bO_2}\rho_{O_2} - fu_{st}$$

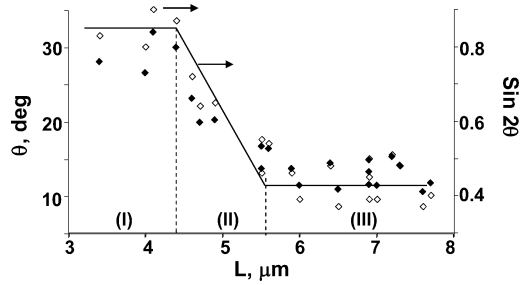

Figure 4. Dependence of angle θ (solid diamonds), which the rod long axis makes with the *XY*-plane, on rod length. L is the real rod length that was calculated as $L_{xy}/\cos\theta$. Line is a guide for eye for sin 2θ vs L data (open diamonds).

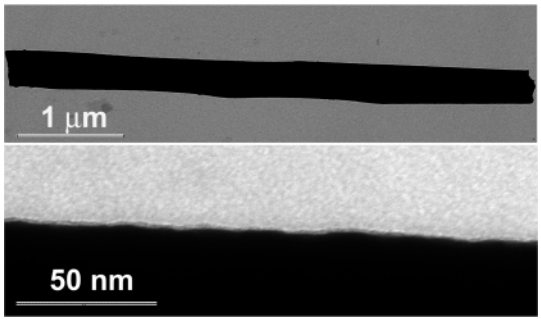

Figure 5. Typical TEM image of a 5 μm long Pt nanorod. At higher resolution, relatively rough surface of the rod wall is clearly seen. This roughness may facilitate oxygen bubbles' nucleation on the walls.

where V_{bO_2} is the bubble volume, ρ the density, g the acceleration due to gravity, f the friction coefficient, $u_{b0} = 0$ the starting bubble velocity, and u_{bst} the steady-state bubble velocity, which is developed during time interval Δt. The steady-state velocity is given by

$$u_{bst} = 2ga^2(\rho_{H_2O} - \rho_{O_2})/9\kappa\eta_{H_2O} = 0.33ga^2(\rho_{H_2O} - \rho_{O_2})/\eta_{H_2O} \quad (1)$$

where a is the bubble radius, η the dynamic viscosity, and $\kappa = {}^2/_3$ is the Rybczynski−Hadamard correction factor for fluid spheres.[22]

A push by water flux caused by the bubbles' departure is a normal force exerted on a nanorod (F_r), which drives its displacement (Figure 6a). Water flux velocity $u_{(H_2O)N}$ equals steady-state velocity of the bubbles in the direction normal to the nanowire surface or

$$u_{(H_2O)N} = u_{bstN} = u_{bst}\cos\theta \quad (2)$$

A balance of forces acting on a nanorod in a H_2O_2−H_2O solution is

$$V_r\rho_r(u_{r0N} - u_{rN})/\Delta t = F_r - F_{drag} \quad (3)$$

u_{r0N} and u_{rN} being starting and final rod velocity in the direction normal to the rod long axis.

As shown in Figure 6a, the $\mathbf{F}_r$ vector can be resolved into two components, one of which is parallel to the *XY*-plane ($F_{r(xy)}$) and the other lies along the direction of gravity, z ($F_{r(z)}$). The component $F_{r(xy)} = F_r \sin\theta$ is responsible for the directional nanorod movement seemingly parallel to the glass surface, which is observed with the microscope. The $F_{r(z)}$ component can, in principle, affect angle θ, thus changing θ-dependent parameters. However, its effect may be compensated by the buoyancy force exerted on the oxygen-covered surface of the bottom hemicylinder of the rod. For simplicity reason, we further neglect force balance changes along z-axis and consider only forces acting parallel to the *XY*-plane.

Upon colliding, the rod and H_2O flux move with the final velocity of the rod, $\mathbf{u}_r$. Momentum conservation requires

$$V_{H_2O}\rho_{H_2O}u_{H_2O} + V_r\rho_r u_{r0} = V_{H_2O}\rho_{H_2O}u_r + V_r\rho_r u_r \quad (4)$$

From eqs 3 and 4 we obtain

$$V_r\rho_r(u_r - u_{r0})/\Delta t = V_{H_2O}\rho_{H_2O}(u_{H_2O} - u_r)/\Delta t - F_{drag} \quad (5)$$

where u_r and u_{r0} are axial velocity components parallel to the *XY*-plane and

$$u_{H_2O} = u_{(H_2O)N}\sin\theta = 0.5u_{bst}\sin 2\theta \quad (6)$$

Hydrodynamic drag on a moving nanorod in the direction parallel to the glass surface can be roughly approximated as[16]

$$F_{drag(xy)} = F_{drag}\sin\theta = 4\pi\eta_{H_2O}u_r L[\ln(L/R) + 0.5]^{-1} \quad (7)$$

L and R being the rod length and radius and $u_r = u_{rN}\sin\theta$.

From the scheme in Figure 6a (bottom), one can suggest that the water push responsible for directional rod motion are generated by oxygen bubbles departing only from the top part of cylindrical rod surface. The bubbles departing from the opposite side surfaces of the cylinder compensate each other and do not contribute significantly to the directional rod movement. Bubbles' departure from the upper tip of the rod generates a force with xy-component directed opposite to $F_{r(x,y)}$. Generally, this force can be neglected because surface area of the tip is much smaller than that of the walls. Bubbles' departure from the bottom hemicylinder and the tip is not favored by the force balance. Unless the rod revolves around its long axis, this surface should remain covered with bubbles, which blocks generating new oxygen. However, real behavior of the gas-evolving nanoscale cylinders suspended in a solution is not known, and we consider total area of rod walls as catalytically active surface responsible for the directional motion.

At low Reynolds numbers, $\sim 10^{-5}$ in our case, inertia plays no role, and a rod moves as long as the force (i.e., water push) acts.[6] In general, axial velocity of a rod can fluctuate in the range $0-u_r$ with frequency and amplitude ($u_{r0} - u_r$) determined by the frequency of the bubble departure events, i.e., rate of the oxygen bubbles' growth. For rods with low catalytic activity of the wall surface (or at very low peroxide concentrations), the water pushes occur rarely, the rod moves by fits and starts, and contribution of the Brownian component is significant. The directionality, therefore, is low, and axial motion is slow. For active catalytic surfaces, bubble growth rate is high enough, the bubbles' departures (and, hence, the water pushes) occur often, the axial motion becomes continuous, and the rod axial velocity attains virtually constant value. Both these types of rod motion were observed experimentally. The latter type may be treated as the case of dynamic equilibrium, and all equations shown below are derived for the continuous rod motion.

Combining eqs 1, 5, 6, and 7 gives

$$F_{r(xy)} = F_{drag(xy)} = V_{H_2O}\rho_{H_2O} \times [0.165ga^2(\rho_{H_2O} - \rho_{O_2})/\eta_{H_2O}\sin 2\theta - u_r]/\Delta t = 4\pi\eta_{H_2O}u_r L[\ln(L/R) + 0.5]^{-1} \quad (8)$$

V_{H_2O} equals volume of the departed oxygen bubbles. Apparently, $V_{H_2O} = v\Delta t$, where v is the rate of oxygen evolution from the rod surface.

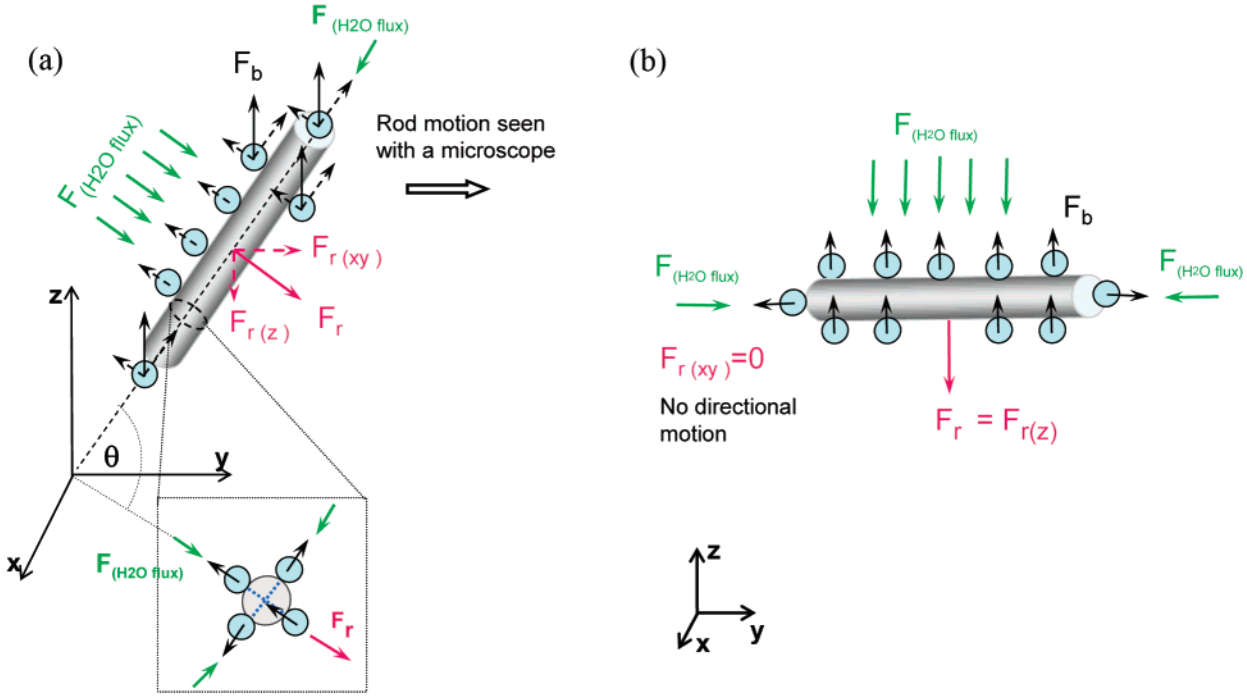

Figure 6. Schematic representation of forces acting on a nanorod (F_r) catalyzing oxygen formation in aqueous H_2O_2 solution. (a) Rod long axis makes angle θ with *XY*-plane. (b) Rod long axis is parallel to *XY*-plane. F_b is the buoyancy force exerted on O_2 bubbles, which is resolved into two components normal and parallel to the rod surface. F_{H_2O} is the push by water flux caused by the bubbles' departure.

For a single nanorod, whose motion is tracked during relatively short time intervals ($\leq$1 min), the reaction rate can be considered constant in time. The reaction rate was determined experimentally by measuring volume of oxygen evolved from a known area of the planar Pt surface, which was prepared by electrochemical deposition under the electroplating conditions identical to those used for Pt rods' preparation. The reaction rate was found to be proportional to the Pt surface area, *S*, and concentration of H_2O_2 ($C_{H_2O_2}$). It can be expressed as

$$\nu = dV_{O_2}/dt = kC_{H_2O_2}S$$

where *k* is the rate constant estimated at $\sim 5 \times 10^{-6}$ m^4/(kg s).

For a single rod

$$\nu = dV_{O_2}/dt = kC_{H_2O_2}2\pi RL \quad (9)$$

Replacing V_{H_2O} by $\nu\Delta t$ and combining eqs 8 and 9, one can calculate steady-state axial velocity of the rod in *XY*-plane

$$u_r^{-1} = (\sin 2\theta)^{-1}\{K_1 + C_{H_2O_2}^{-1}K_2[kR(\ln(L/R) + 0.5)]^{-1}\} \quad (10)$$

where $K_1 = \eta_{H_2O}[0.165ga^2(\rho_{H_2O} - \rho_{O_2})]^{-1}$ and $K_2 = 12.1\eta_{H_2O}^2[ga^2\rho_{H_2O}(\rho_{H_2O} - \rho_{O_2})]^{-1}$. For $T = 300$ K, the coefficients K_1 and K_2 can be written as

$$K_1 = 0.55 \times 10^{-6}a^{-2}\ (\text{s m}^{-1}); \quad K_2 = 10^{-12}a^{-2}\ (\text{m})$$

Assessment of Gravitational Model Fit to the Experimental Data. The experimentally measured dependencies of rod axial velocity on *L* and $C_{H_2O_2}$ satisfy eq 10. One can see that u_r is proportional to sin 2θ, $C_{H_2O_2}$, *k*, *R*, and [ln(*L*/*R*) + 0.5]. The proportionality of rod axial velocity to sin 2θ explains qualitative similarity of the u_r vs *L* and sin 2θ vs *L* graphs shown in Figures 2 (left) and 4. The direct dependence of wire velocity on its length is determined by the only term [ln(*L*/*R*) + 0.5].[23] In the wire length ranges of 2−3, 3−4, and 4−6 μm, the logarithmic term increases by ~13%, 8%, and 10%, respectively. Such slow growth makes wire velocity virtually independent of rod length within the dispersion range of the experimental points, which is observed for regions I and III in Figure 2 (left). The sharp decrease in rods' velocity in the region II can only be explained by the similar decrease in sin 2θ (Figure 4). Hence, the major effect of the rod length on its velocity is indirect and occurs through the change of the tilt angle θ with length. When the rod long axis is parallel to *XY*-plane, sin 2θ = 0 and u_r = 0. Because the probability of the almost parallel rod orientation in solution is about 30% (see, e.g., Figure 3, the rod on the right), it may be one of several reasons why not all catalytic rods have the appreciable axial velocity (see, e.g., Supporting Information movie 1).

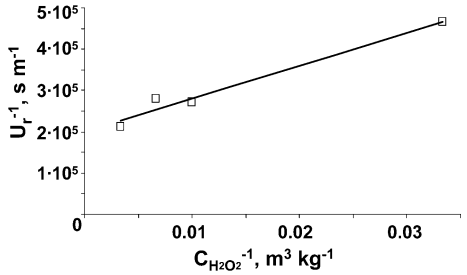

Figure 7. Axial velocity of ~4.5 μm long rods in the coordinate system of eq 10.

A plot of the experimental data in the u_r^{-1} vs $C_{H_2O_2}^{-1}$ coordinate system shows good linearity (Figure 7) and, for ~4.5 μm long Pt rods, can be described by the equation

$$u_r^{-1} = 8.0 \times 10^6 C_{H_2O_2}^{-1} + 2.0 \times 10^5$$

Rough estimating of average size of the oxygen bubbles (a) from $K_1(\sin 2\theta)^{-1} = 2.0 \times 10^5$ yields a ~2 μm, which seems a reasonable value relative to the rod size, and is comparable to the size of the bubbles observed on nanorods resting on the glass surface (see, e.g., Supporting Information movie 4). To

make further quantitative predictions using the graph slope is challenging because of uncertainty in the reaction constant for a single catalytic rod, k. It is very possible that catalytic activity of nanorods is much higher than activity of the planar surface. Determination of k by direct measurement of oxygen evolution from a nanorod suspension in H_2O_2 also gives a very rough estimate because of uncertainty in the number of oxygen-producing rods in the suspension. Reliable measurement of catalytic properties of a single particle is, in principle, not achievable with conventional methods that give statistically averaged data.

Although dependence of the rod axial velocity on rod radius, R, was not studied in this work, literature data showed that decreasing rod diameter led to much slower rods' motion,[1] which is in agreement with eq 10.

In the majority of cases, the rods' trajectories are almost linear (Figure 1a), which is expected for the bubbles' departure mainly from the top part of cylindrical rod surface and mutual compensation of the bubbles departing from the opposite side walls of the cylinder (Figure 6a, bottom). However, if the frequency of the bubble departure events is different on the opposite sides of cylindrical rod surface, it creates a additional side force, which may cause side drift and/or rod rotation around the short axis. In combination with the linear motion this side force results in a circular rod trajectory (Figure 1b and movie 1). When the linear motion is hindered (i.e., the lower rod end stuck to the glass slide or two rods are crossed), the side force leads to rods' rotation (Figure 1c,d and movies 2, 3).

Bubbles' departure from the upper tip of the tilted rod generates a force with xy-component directed opposite to $F_{r(xy)}$ (Figure 6a). At high θ values of shorter rods, $F_{r(xy)}$ is relatively large, and the contribution of this force is insignificant because surface area of the tip is much smaller than that of the cylindrical rod surface. However, at low θ values of longer rods, $F_{r(xy)}$ becomes smaller, and the contribution of the force acting on the upper rod tip becomes more pronounced, which can lower directionality. The above-described side force, when exists, can also contribute to the directionality decrease. This may be a reason for the experimentally observed decrease in directionality with rod length (Figure 2, bottom left). Here again, influence of rod length is indirect and occurs through the change in the θ value.

5. Conclusions

In summary, monocomponent Pt and Rh nanorods self-propel in aqueous solutions of hydrogen peroxide due to H_2O_2 catalytic decomposition to water and oxygen on the rod surface. To explain this phenomenon, we present a model that is based on oxygen bubbles' evolution from the rod surface and related gravitational forces. The model considers rod motion in the 3D space to account for nonparallel rods' orientation relative to the horizontal plane. Such orientation has been shown to play a major role in rods' propulsion. Momentum exchange between such a "tilted" rod and water flux, caused by the oxygen bubbles' departure from the rod surface, drives the directional motion of the rod. The complex nonlinear dependence of rod's axial velocity on its length can only be explained by the similar dependence of the angle, which rod's long axis makes with XY-plane, on rod's length. The proposed model is in good qualitative agreement with experimental data and, in some cases, allows even semiquantitative conclusions to be drawn.

In aqueous H_2O_2 solutions, hydrodynamic behavior of the monometallic nanorods is similar to that of bimetallic rods and some larger particles of different composition[9] that catalyze oxygen formation. The mono- and bicomponent rods have similar motion trajectories and comparable values of axial velocity and directionality. Such similarity, which is observed in the same reaction media, allows to suggest that the propulsion mechanisms of these particles should be essentially the same. There is no need in two or more metal components to cause the directional rod motion, and hence, mechanisms that heavily rely on chemical asymmetry of the rod surface seem less likely to exist. However, the presence of another metal in the bimetallic nanorods may increase catalytic activity of the system (and hence axial velocity) due to electrochemically induced electron redistribution.[13] In addition, the bimetallic rods with considerably different catalytic activity of the metal components may have larger angle θ (and again higher axial velocity) because of different buoyancy forces exerted on the oxygen-evolving and inactive parts of the rod's body. (Supporting Information movie 4 clearly shows that only the catalytically active rod end is covered with oxygen bubbles.) For example, formation of a 30 nm thick O_2 film on the catalytically active end increases the buoyancy force by 44%. For these asymmetric rods, the active end covered with oxygen bubbles is most likely to be the upper one. According to the scheme in Figure 6a, the rods always move the upper end first, which may offer an explanation for experimentally observed motion of the bimetallic rods active end first.[1,13]

In principle, the proposed here gravitational model may be applicable to various rodlike nanoparticles that catalyze gas-formation reactions. However, high-aspect-ratio monocomponent particles are probably the simplest class of nanomotors that can work in this medium. For geometrically isotropic particles, the presence of a second (inactive) surface component is needed to enable directional motion. Further steps toward controlled nanomachinery systems may exploit geometric asymmetry of hetero-nanostructures composed of several metallic and/or nonmetallic parts with different chemical and physical properties. The judicious design of more complex asymmetric multicomponent architectures may lead to more sophisticated trajectory patterns as was shown for larger scale catalytic systems containing a large fraction of inactive components.[3,8,11]

Acknowledgment. Confocal microscopy was done at the Center for Quantitative Cell Analysis at the Huck Institutes of the Life Sciences, Penn State University. I thank Elaine Kunze for help with confocal imaging. XPS, AES, and ICP analysis was conducted at the Materials Characterization Laboratory at Penn State University. I am grateful to Tom Mallouk and Darrell Velegol for fruitful discussions. This work has been partially supported by NSF MRSEC, DMR-021362.

Supporting Information Available: Real-time videos of monocomponent Pt (1−3) and bicomponent (4) nanorods and 300 μm thick Pt wire (5) submerged in an aqueous H_2O_2 solution. This material is available free of charge via the Internet at http://pubs.acs.org.

References and Notes

(1) Paxton, W. F.; Kistler, K. C.; Olmeda, C. C.; Sen, A.; St. Angelo, S. K.; Cao, Y.; Mallouk, T.; Lammert, P. E.; Crespi, V. H. *J. Am. Chem. Soc.* **2004**, *126*, 13424.

(2) (a) Fournier-Bidoz, S.; Arsenault, A. C.; Manners, I.; Ozin, G. A. *Chem. Commun.* **2005**, 441. (b) Ozin, G. A.; Manners, I.; Fournier-Bidoz, S.; Arsenault, A. *Adv. Mater.* **2005**, *17*, 3011.

(3) He, Y.; Wu, J.; Zhao, Y. *Nano Lett.* **2007**, *7*, 1369.

(4) Howse, J.; Jones, R.; Ryan, A.; Gough, T.; Vafabakhsh, R.; Golestanian, R. *Phys. Rev. Lett.* **2007**, *99*, 048102.

(5) Su, M.; Dravid, V. *Nano Lett.* **2005**, *5*, 2023.

(6) (a) Berg, H. C.; Anderson, R. A. *Nature (London)* **1973**, *245*, 380. (b) Silverman, M.; Simon, M. *Nature (London)* **1974**, *249*, 73. (c) Purcell, E. M. *Am. J. Phys.* **1977**, *45*, 3.

(7) Dreyfus, R.; Baudry, J.; Roper, M.; Fermigier, M.; Stone, H.; Bibette, J. *Nature (London)* **2005**, *437*, 862.

(8) Ismagilov, R. F.; Schwartz, A.; Bowden, N.; Whitesides, G. M. *Angew. Chem., Int. Ed.* **2002**, *41*, 652.

(9) Vicario, J.; Eelkema, R.; Browne, W. R.; Meetsma, A.; La Crois, R. M.; Feringa, B. L. *Chem. Commun.* **2005**, *31*, 3936.

(10) Dhar, P.; Fischer, Th. M.; Wang, Y.; Mallouk, T. E.; Paxton, W. F.; Sen, A. *Nano Lett.* **2006**, *6*, 66.

(11) Catchmark, J. M.; Subramanian, S.; Sen, A. *Small* **2005**, *1*, 202.

(12) Paxton, W. F.; Sen, A.; Mallouk, T. *Chem.—Eur. J.* **2005**, *11*, 6462.

(13) Wang, Y.; Hernandez, R. M.; Bartlett, D. J., Jr.; Bingham, J. M.; Kline, T. R.; Sen, A.; Mallouk, T. E. *Langmuir* **2006**, *22*, 10451.

(14) Lappa, M. *Fluids, Materials and Microgravity*; Elsevier: Amsterdam, 2004.

(15) Van de Ven, T. *Colloidal Hydrodynamics*; Academic Press: London, 1989; Chapter 3(2).

(16) Happel, J.; Brener, H. *Low Reynolds Number Hydrodynamics*; Martinus Nijhoff Publishers: Dordrecht, 1986; Chapter 5(11).

(17) St. Angelo, S.; Waraksa, C.; Mallouk, T. *Adv. Mater.* **2003**, *15*, 402.

(18) Schumb, W.; Satterfield, W. C.; Wentworth, R. L. *Hydrogen Peroxide*; Reinhold: New York, 1955.

(19) Uri, N. *Chem. Rev.* **1952**, *50*, 375.

(20) Sheldon, R.; Kochi, J. In *Advances in Catalysis*; Eley, D., Pines, H., Weisz, P., Eds.; Academic Press: New York, 1976.

(21) Van Stralen, S.; Cole, R. *Boiling Phenomena*; Hemisphere Publ. Corp.: Washington, 1979; Vol. 1.

(22) Morrison, I.; Ross, S. *Colloidal Dispersions*; Wiley: New York, 2002; p 288.

(23) Because both the drag and the oxygen formation rate are proportional to rod length, the term L does not appear in the final equation.